Thermochromism of Model Organic Aerosol Matter

ARTICLE *in* JOURNAL OF PHYSICAL CHEMISTRY LETTERS · DECEMBER 2010

Impact Factor: 7.46 · DOI: 10.1021/jz900186e · Source: OAI

4 AUTHORS:

Angela G. Rincon
University of Cambridge
55 PUBLICATIONS **1,702** CITATIONS
SEE PROFILE

Marcelo I. Guzman
University of Kentucky
60 PUBLICATIONS **705** CITATIONS
SEE PROFILE

Michael R. Hoffmann
California Institute of Technology
379 PUBLICATIONS **30,162** CITATIONS
SEE PROFILE

Agustin J Colussi
California Institute of Technology
214 PUBLICATIONS **4,224** CITATIONS
SEE PROFILE

THE JOURNAL OF PHYSICAL CHEMISTRY Letters

pubs.acs.org/JPCL

Thermochromism of Model Organic Aerosol Matter

Angela G. Rincón, Marcelo I. Guzmán,† M. R. Hoffmann, and A. J. Colussi*

W. M. Keck Laboratories, California Institute of Technology, Pasadena, California 91125

ABSTRACT Laboratory experiments show that the optical absorptivity of model organic matter is not an intrinsic property, but a strong function of relative humidity, temperature, and insolation. Suites of representative polyfunctional $C_xH_yO_z$ oligomers in water develop intense visible absorptions upon addition of inert electrolytes. The resulting mixtures reach mass absorption cross sections σ(532 nm) $\sim$ 0.1 m^2/gC in a few hours, absorb up to 9 times more solar radiation than the starting material, can be half-bleached by noon sunlight in $\sim$1 h, and can be repeatedly recycled without carbon loss. Visible absorptions red-shift and evolve increasingly faster in subsequent thermal aging cycles. Thermochromism and its strong direct dependences on ionic strength and temperature are ascribed to the dehydration of >CH−C(OH)< groups into >C=C< unsaturations by a polar E1 mechanism, and bleaching to photoinduced retrohydration. These transformations are deemed to underlie the daily cycles of aerosol absorption observed in the field, and may introduce a key feedback in the earth's radiative balance.

SECTION Atmospheric, Environmental and Green Chemistry

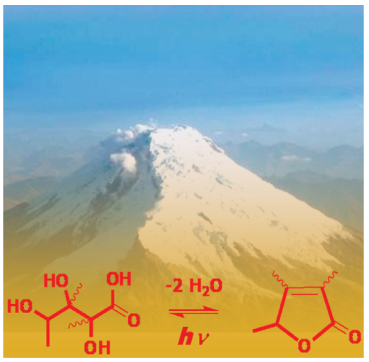

Atmospheric aerosols, by backscattering solar radiation, attenuate the full impact of greenhouse gases.[1] However, by absorbing sunlight, they warm the upper troposphere, thereby affecting its thermal stability, melting the mountain glaciers that feed major rivers, and reducing the persistence and reflectance of clouds.[2−7] Clinical and epidemiological studies reveal that aerosols also induce detrimental health effects.[8−10] More than half of the mass of tropospheric aerosols consists of complex organic matter (OM)[11−13] largely derived from the chemical transformation of (natural and anthropogenic) gas emissions into species that can attach to seed particles.[14,15] OM is one of the main contributors to aerosol absorptivity in the near-UV−visible ranges.[16−19] Although full chemical speciation might be required to unravel OM toxicology, the optical properties of OM relevant to the earth's radiative balance should be common to functionally related mixtures.[6,20−24]

The processes that control OM chemical composition remain speculative. Even how simple gases and vapors attach to aerosol surfaces is not well understood.[25,26] The notion of attachment via physical condensation has motivated much research focused on gas-phase reactions leading to low-volatility organics.[26] However, overall gas uptake onto large surface-to-volume ratio microparticles can exceed the limits imposed by gas/bulk liquid partition coefficients[27] and, moreover, be enhanced by fast reactions on aerosol surfaces.[28] Gaseous species may take part in bulk liquid reactions only after being effectively incorporated into the aerosol through the interface.[29−35] Furthermore, since airborne aerosol particles are exposed to intense sunlight half of the time, interfacial or condensed-phase photochemical reactions must participate in the processing of OM.[21] Note that photochemistry in concentrated aerosol-phase media, at variance with gas-phase photochemistry, is not necessarily degradative. Organic photochemistry in tropospheric aerosol particles exposed to $\lambda > 300$ nm sunlight likely involves conjugated carbonyl chromophores.[21] In fact, the endothermic and necessarily exentropic accretion of carbonyl groups $\{\Delta H_f[CO-(C)_2] = -31.4$ kcal mol$^{-1}\}$ into (poly)ethers $\{\Delta H_f[O-(C)_2] = -23.2$ kcal mol$^{-1}\}$[36] should be ideally driven by the free energy of absorbed photons.[37,38] In this Letter we report the dramatic effect of strong electrolytes, such as those present in atmospheric aerosol droplets, on the optical properties of representative model OM produced by photolysis of the environmentally ubiquitous α-dicarbonyl pyruvic acid (PA).[20] We evaluate OM mass absorption cross sections and Armstrong exponents after thermal and photochemical treatments under realistic conditions, and estimate the associated changes in absorbed solar energy fluxes.

Figure 1 shows UV−visible absorption spectra of (A) an aqueous 80 mM PA in 2 M ammonium bisulfate (ABS) solution at pH 1.0 before photolysis and after each of the following successive steps, (B) photolysis under continuous air sparging for 4.5 h, (C) thermal aging in the dark at 60 °C in stoppered cuvettes for 72 h, and (D) rephotolysis for 4.5 h. Line E is the spectrum of a 80 mM PA solution after stage C in the absence of added ABS. Since similar results are obtained following the addition of ABS to previously photolyzed PA solutions, we infer that ABS actually promotes thermal aging. PA solutions in the presence of Na_2SO_4 or NH_4ClO_4 at pH 1.0 behave similarly (Figure S1, Supporting Information (SI)) revealing that the bathochromic effect of ABS is not specific to sulfate or

Received Date: October 26, 2009
Accepted Date: December 2, 2009

DOI: 10.1021/jz900186e | *J. Phys. Chem. Lett.* **2010**, *1*, 368–373

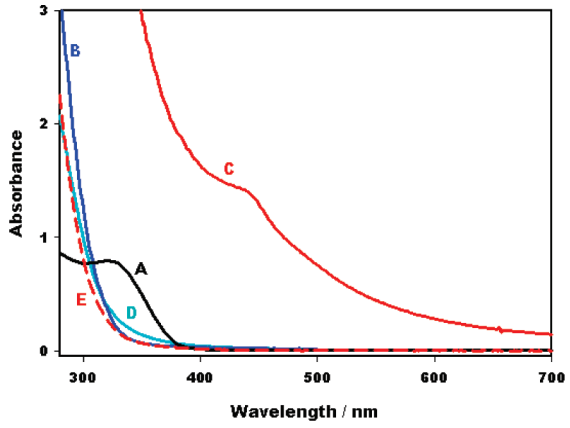

Figure 1. UV−visible absorption spectra of aqueous 80 mM PA in 2 M ABS solutions at pH ∼1. (A) before photolysis; (B) after 4.5 h photolysis; (C) B after 17 h at 25 °C followed by 48 h at 60 °C, in the dark; (D) C after 4.5 h photolysis; (E) A after 17 h at 25 °C followed by 48 h at 60 °C, in the dark, but in the absence of ABS.

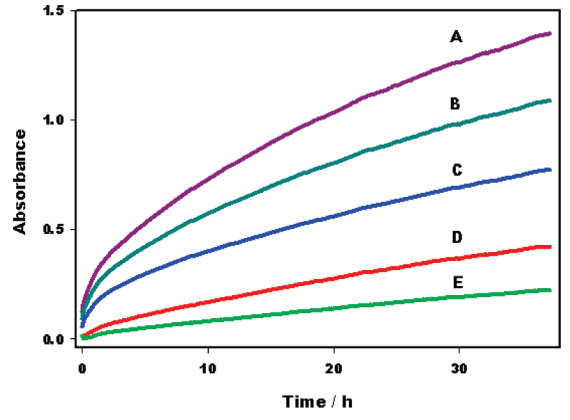

Figure 2. Absorbances A_λ versus time in a 120 mM PA solution previously photolyzed for 4.5 h, after diluting it by half with 4 M ABS, and then maintained at 60 °C. (A) λ/nm = 350; (B) 360; (C) 380; (D) 450; (E) 500. Curves adhere to Kohlrausch kinetics: $A_\lambda(t) = A_\lambda(\infty)\,[1 - \exp(-k_\lambda t)^n]$; $n(\lambda) < 1$ (see text).

ammonium,[31] but shared by other strong electrolytes. Neither sulfate or perchlorate esters are expected to enhance absorptions above $\lambda > 300$ nm.[39] We chose 2 M ABS media because ABS is the major electrolyte found in atmospheric aerosols. Note that 2 M ABS is in equilibrium with water vapor at ∼90% relative humidity (RH), 25 °C, whereas [ABS] exceeds ∼10m below RH ∼65%. Electrolyte effects should be therefore magnified in drier climates or in the upper troposphere.[40,41]

Figure 2 shows how spectral absorbances $A(\lambda)$ develop as functions of time during stage C. Absorbances, $A(\lambda)$, increase as single-exponential growth functions: $A_\lambda(t) = A_\lambda(\infty)\,[1 - \exp(-k_\lambda t)]$, at $\lambda \leq 270$ nm and with stretched exponential (Kohlrausch) kinetics: $A_\lambda(t) = A_\lambda(\infty)\,[1 - \exp(-k_\lambda\, t)^n]$ ($n(\lambda) < 1$), farther to the red (Figures S2 and S3, SI). The dissimilar kinetic behaviors described above suggest that the species responsible for the longer wavelength absorptions do not ensue directly from photolysis products, but through a series of `scaffolding' intermediates of increasing complexity.

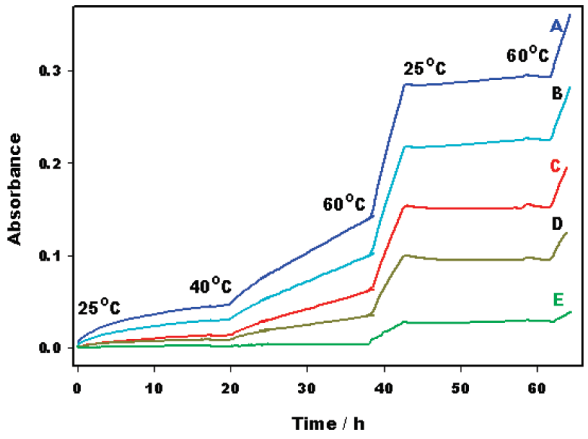

Figure 3. Absorbances A_λ versus time in a previously photolyzed 60 mM PA, 2 M ABS solution, successively aged at various temperatures, as indicated. (A) λ/nm = 380; (B) 400; (C) 450; (D) 480; (E) 550.

The acceleration of initial rates, $[\partial A_\lambda(t)/\partial t]_0$ by 2 M ABS depends sensitively and nonmonotonically on λ. Initial rates are enhanced up to a factor of 150 at $\lambda = 430$ nm in stage C, and up to a factor of 395 at $\lambda = 480$ nm in the second thermal aging treatment after stage D (Figure S4, SI). We infer that the composition of the solution changes subtly but irreversibly upon repeated recycling, although total organic carbon remains constant after the first thermal treatment[20] and UV−visible spectra look alike after every bleaching stage. These changes appear to involve the progressive accumulation of molecular structures more prone to color development.

Figure 3 shows that rates, $\partial A_\lambda(t)/\partial t$, are strong functions of temperature along the course of the reaction. From the observed $\partial A_\lambda(t)/\partial t$ changes upon temperature jumps from 25 to 40 °C, and from 40 to 60 °C, i.e., at the compositions attained after 20 and 38.3 h, respectively, we derive sizable activation energies: $E_{40/25} = 28$ kcal mol^{-1} and $E_{60/40} = 30$ kcal mol^{-1}, without significant λ-dependences. Activation energies derived from initial rates (i.e., immediately after photolysis) at 25 and 60 °C: $E_{a,0} \sim 13$ kcal mol^{-1}, are considerably smaller. We infer that the mechanism of color development changes with time (conversion), as expected from the suggested "scaffolding" scheme.

The products of the photolysis of fluid and frozen aqueous PA solutions have been previously identified by electrospray mass and ^{13}C NMR spectrometries.[21,42,43] They consist of aliphatic mono- or polycarboxylic acids, containing alcohol −OH, aldehyde −C(H)═O, and ether >O groups.[20] Under mild atmospheric conditions, these functionalities should undergo low activation energy reactions in the dark. Aldehydes may self-condense ($E_a \sim 11.0$ kcal mol^{-1}),[30,31,44−46] alcohols may produce olefins ($E_a \sim 30.0$ kcal mol^{-1}),[47] and acids may esterify inter- or intramolecularly, leading to esters and lactones, respectively.[48] Condensations entail the loss of polar groups and also, in the case of olefin formation, the creation of additional unsaturations. Moreover, since olefins are readily hydrated photochemically,[49,50] the chemical consequences of thermal aging could be repeatedly reversed. The dramatic effect of added electrolytes on initial rates

DOI: 10.1021/jz900186e | J. Phys. Chem. Lett. 2010, 1, 368–373

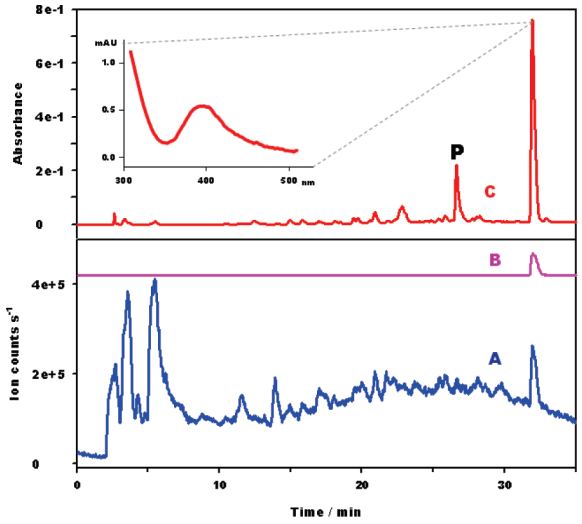

Figure 4. Reversed-phase high-performance liquid chromatography (HPLC) of a photolyzed 80 mM PA, 2 M ABS solution aged in the dark for 2 days at 25 °C. (A) Total negative ion current MS signals; (B) 139 Da negative ion current MS signals; (C) Absorbance at $\lambda = 254$ nm. The inset is the spectrum of the species eluting at 32 min.

(Figure S4, SI) is consistent with the acid-catalyzed dehydration of secondary and tertiary alcohols by an E1 elimination mechanism via carbocations.[51] The appearance of cyclic olefin signals at $\delta(^1H) \sim 7.5$ ppm and $\delta(^{13}C) \sim 125 \pm 10$ ppm in the NMR spectra of thermally aged solutions is consistent with the proposed transformations.[52,53] This phenomenological analysis should apply to chemically related systems of similar complexity, such as aerosol OM.

Figure 4 shows a typical reversed-phase liquid chromatogram of solutions after stage C. The more polar species containing carboxylate groups (i.e., those eluting early on) give rise to the most intense total negative ion count (TIC) mass spectral signals (Figure 4A) and the weakest UV absorptions (Figure 4C). The late, strongly absorbing signals are associated with less polar components (Figure 4C). Species such as those eluting at 32 min, which absorbs into the visible with a maximum at $\lambda \sim 400$ nm, should contribute to the long-wavelength tail of curve C in Figure 1. Figure 4B is the chromatogram reported by negative ion electrospray mass spectroscopy (ES-MS) tuned to $m/z = 139$. High-resolution ES-MS analysis reveals that this peak corresponds to the $C_6H_3O_4$ molecular formula (mass 139.0031 Da) tentatively assigned to the anion of coumalic acid (Scheme S1, SI). Figure 5 shows the negative TIC mass spectra of the species eluting simultaneously with peak `P' in Figure 4C. The plethora of ion signals in the $m/z = 50$ to 2000 range gives an indication of the overall composition of a mixture whose extreme complexity is not fully resolved under the present analytical conditions. It also demonstrates that low-polarity and poor ionization ability are apparently necessary but insufficient conditions for high absorptivity in this model system.[54] A normal distribution regression to ion signal intensities (yellow trace, Figure 5) has a maximum at $m/z = 381$, which translates into an average mass: $\langle m \rangle = 433$ Da (cf. 88 Da for PA, the starting material).

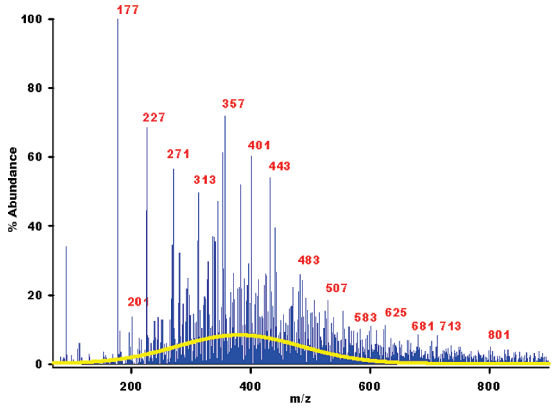

Figure 5. Negative ion ES-MS spectrum of the peak P eluting at 26.8 min in Figure 4. The yellow trace corresponds to a Gaussian regression curve centered at 381 Da.

The processing of 80 mM PA solutions reduces the total organic carbon content to ~30% of the initial value at stage C; it remains constant thereafter.[20] Hence, processed solutions contain ~0.86 gC L^{-1}. From the absorbance of the thermally aged mixture at $\lambda = 532$ nm (Figure 1, curve C): $A(532\text{ nm}) = 0.60 = \sigma(532\text{ nm}) \times l \times [C]$, where $l = 0.01$ m, and $[C] = 860$ gC m^{-3}, we obtain a mass absorption cross section: $\sigma(532\text{ nm}) \sim 0.07$ m^2/gC. This value, which is within an order of magnitude of the estimated mass absorption cross section of the ("brown") organic carbon component of fully aged aerosols over Mexico City,[19] is expected to increase substantially in more concentrated aerosols due to the onset of supramolecular interactions.[20] The main point, however, is that present results show that $\sigma(\lambda)$ values are not intrinsic to a given aerosol specimen, but depend on its history. RH, by regulating the ionic strength of the aerosol, should have a strong effect on color intensity and development rates. The low RH prevalent at high altitudes should magnify the importance of absorption relative to scattering.

Figure 6 contains log−log plots of $\sigma(\lambda)$ for bleached and thermally aged PA/ABS solutions, as well as spectral solar energy fluxes $\phi(\lambda)$ (in J s^{-1} m^{-2} nm^{-1}) at the Earth's surface at zero zenith angle.[16] From this information we can calculate the Armstrong exponents, α, and the ratio of absorbed solar energy fluxes by the aged (C) and bleached (stages B or D in our experiments) model organics, γ, eqs 1 and 2:

$$\sigma(\lambda) = \beta\lambda^{-\alpha} \quad (1)$$

$$\gamma = \frac{\int_{300}^{700} \sigma_C(\lambda)\phi(\lambda)d\lambda}{\int_{300}^{700} \sigma_B(\lambda)\phi(\lambda)d\lambda} \quad (2)$$

We obtain $\alpha_C = 5.3$, $\alpha_B = 8.7$, and $\gamma = 8.9$ from Figure 6, and $\alpha_C = 5.2$, $\alpha_D = 10.9$, and $\gamma = 9.6$ from Figure S5 (see SI). Note that the $\alpha_C \sim 5.3$ value, which is reproduced after thermal treatments, is comparable to those reported for biomass-burning-derived aerosols.[18] We also found that the longer wavelength absorptions of thermally aged solutions disappear faster than those below $\lambda \sim 350$ nm during photobleaching. The net effect is that absorbed solar energy fluxes decrease with biexponential kinetics by 50% in ~50 min

DOI: 10.1021/jz900186e | J. Phys. Chem. Lett. 2010, 1, 368–373

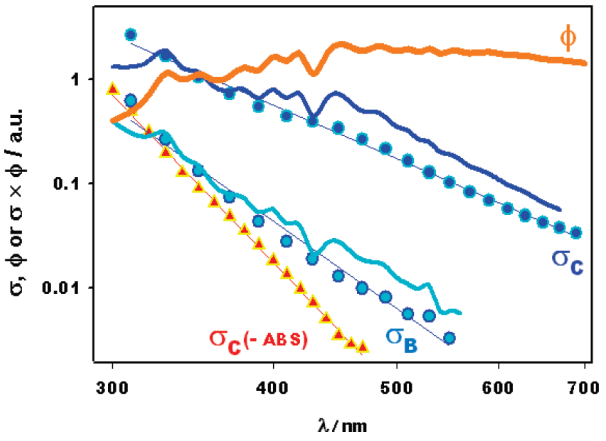

Figure 6. Solar energy fluxes $\phi(\lambda)$ at the earth's surface at zero zenith angle (bold orange curve). Absorption cross sections $\sigma(\lambda)$ and $\sigma(\lambda) \times \phi(\lambda)$ products for a 60 mM PA, 2 M ABS solution, after 4.5 h photolysis [$\sigma_B(\lambda)$, cyan circles], [$\sigma_B(\lambda) \times \phi(\lambda)$, bold cyan curve], followed by thermal treatment as in Figure 3 [$\sigma_C(\lambda)$, blue circles], [$\sigma_C(\lambda) \times \phi(\lambda)$, bold blue curve]. σ_C(−ABS) corresponds to stage C in experiments performed in the absence of ABS (red triangles).

under 1 sun (1 sun is equivalent to 627 W m^{-2} solar irradiance between 300 and 700 nm)[17] (Figure S6, SI). These phenomena, and their time scales are consistent with the diel cycles of aerosol scattering and absorption observed over Mexico City at constant total carbon (15 ± 5) μg m^{-3} loadings. Aerosol absorptivity peaks early in the morning and reaches minimum values past noon, i.e., under conditions of maximum photochemical processing, whereas scattering peaks ~4 h later.[55,56] Our results suggest that σ intensification at night time may be due to browning reactions in the aerosol phase, and σ reduction during daytime may be the result of photobleaching. Although changes in black carbon emissions and meteorology could also contribute to these phenomena, absorption of solar radiation by brown carbon aerosol should be expected to be strongly modulated by environmental conditions, such as temperature and RH.

Aqueous PA (98%, bidistilled at reduced pressure) solutions (3.5 mL) were photolyzed (typically for 4.5 h, at 293 K under continuous air sparging) in fused silica cuvettes (1 cm optical path) with light from a 1 kW high pressure Xe−Hg lamp through tandem water and 305 nm long-pass filters. The cuvettes were immediately stoppered after photolysis and placed in the temperature-controlled holder of a UV−visible absorption spectrophotometer for thermal aging. Aged solutions were rephotolyzed while being sparged with air at 293 K, and otherwise reprocessed over similar cycles. Commercial ABS, sodium sulfate, and ammonium perchlorate were used as received. All solutions were made in deionized, ultrapure water (resistivity 18.2 MΩ cm) from a Millipore purification system. Sulfuric acid (1 M) was used to adjust the pH of the solutions. Salts were added to PA solutions prior to, or immediately after photolysis, as indicated. Further details may be found in previous publications from our laboratory,[20,21] and in Chemicals and Procedures, SI.

SUPPORTING INFORMATION AVAILABLE

Additional data and experimental details. This material is available free of charge via the Internet at http://pubs.acs.org.

AUTHOR INFORMATION

Corresponding Author:

*To whom correspondence should be addressed.

Present Addresses:

† Current address: School of Engineering and Applied Sciences, Harvard University, Cambridge, Massachusetts 02138.

ACKNOWLEDGMENT This project was financially supported by the National Science Foundation (ATM-0714329). A.G.R. acknowledges financial support from the Swiss National Science Foundation (PBL2-110274).

REFERENCES

(1) Alexander, D. T. L.; Crozier, P. A.; Anderson, J. R. Brown Carbon Spheres in East Asian Outflow and Their Optical Properties. *Science* **2008,** *321*, 833–836.

(2) Ghan, S. J.; Schwartz, S. E. Aerosol Properties and Processes - A Path from Field and Laboratory Measurements to Global Climate Models. *Bull. Am. Meteorol. Soc.* **2007,** *88*, 1059–1083.

(3) Flanner, M. G.; Zender, C. S.; Hess, P. G.; Mahowald, N. M.; Painter, T. H.; Ramanathan, V.; Rasch, P. J. Springtime Warming and Reduced Snow Cover from Carbonaceous Particles. *Atmos. Chem. Phys.* **2009,** *9*, 2481–2497.

(4) Ramanathan, V.; Feng, Y. On Avoiding Dangerous Anthropogenic Interference with the Climate System: Formidable Challenges Ahead. *Proc. Natl. Acad. Sci. U.S.A.* **2008,** *105*, 14245–14250.

(5) Fan, J. W.; Zhang, R. Y.; Tao, W. K.; Mohr, K. I. Effects of Aerosol Optical Properties on Deep Convective Clouds and Radiative Forcing. *J. Geophys. Res.* **2008,** *113*, D08209, DOI: 10.1029/2007jd009257.

(6) Dinar, E.; Riziq, A. A.; Spindler, C.; Erlick, C.; Kiss, G.; Rudich, Y. The Complex Refractive Index of Atmospheric and Model Humic-Like Substances (HULIS) Retrieved by a Cavity Ring Down Aerosol Spectrometer (CRD-AS). *Faraday Discuss.* **2008,** *137*, 279–295.

(7) Zhang, H.; Wang, Z. L.; Guo, P. W.; Wang, Z. Z. A Modeling Study of the Effects of Direct Radiative Forcing Due to Carbonaceous Aerosol on the Climate in East Asia. *Adv. Atmos. Sci.* **2009,** *26*, 57–66.

(8) Enami, S.; Hoffmann, M. R.; Colussi, A. J. Acidity Enhances the Formation of a Persistent Ozonide at Aqueous Ascorbate/Ozone Gas Interfaces. *Proc. Natl. Acad. Sci. U.S.A.* **2008,** *105*, 7365–7369.

(9) Li, N.; Wang, M. Y.; Bramble, L. A.; Schmitz, D. A.; Schauer, J. J.; Sioutas, C.; Harkema, J. R.; Nel, A. E. The Adjuvant Effect of Ambient Particulate Matter Is Closely Reflected by the Particulate Oxidant Potential. *Environ. Health Perspect.* **2009,** *117*, 1116–1123.

(10) Lippmann, M. Health Effects of Airborne Particulate Matter. *New Eng. J. Med.* **2007,** *357*, 2395–2397.

(11) Andreae, M. O.; Gelencser, A. Black Carbon or Brown Carbon? The Nature of Light-Absorbing Carbonaceous Aerosols. *Atmos. Chem. Phys.* **2006,** *6*, 3131–3148.

DOI: 10.1021/jz900186e | *J. Phys. Chem. Lett.* **2010,** *1*, 368–373

(12) Graber, E. R.; Rudich, Y. Atmospheric HULIS: How Humic-Like Are They? A Comprehensive and Critical Review. *Atmos. Chem. Phys.* **2006,** *6*, 729–753.
(13) Hallquist, M.; Wenger, J C.; Baltensperger, U.; Rudich, Y.; Simpson, D.; Claeys, M.; Dommen, J.; Donahue, N. M.; George, C.; Goldstein, A. H.; Hamilton, J. F.; Herrmann, H.; Hoffmann, T.; Iinuma, Y.; Jang, M.; Jenkin, M. E.; Jimenez, J. L.; Kiendler-Scharr, A.; Maenhaut, W.; McFiggans, G.; Mentel, Th. F.; Monod, A.; Prevot, A. S. H.; Seinfeld, J. H.; Surratt, J. D.; Szmigielski, R.; Wildt, J. The Formation, Properties and Impact of Secondary Organic Aerosol: Current and Emerging Issues. *Atmos. Chem. Phys.* **2009,** *9*, 5155–5236.
(14) Adachi, K.; Buseck, P. R. Internally Mixed Soot, Sulfates, and Organic Matter in Aerosol Particles from Mexico City. *Atmos. Chem. Phys.* **2008,** *8*, 6469–6481.
(15) Garland, R. M.; Ravishankara, A. R.; Lovejoy, E. R.; Tolbert, M. A.; Baynard, T. Parameterization for the Relative Humidity Dependence of Light Extinction: Organic-Ammonium Sulfate Aerosol. *J. Geophys. Res.* **2007,** *112*, D19303, DOI: 10.1029/2006jd008179 .
(16) Finlayson-Pitts, B. J.; Pitts, J. N., Jr. *Chemistry of the Upper and Lower Atmosphere*; Academic Press: San Diego, CA, 2000.
(17) Seinfeld, J. H.; Pandis, S. N. *Atmospheric Chemistry and Physics: from Air Pollution to Climate Change*, 2nd ed.; Wiley: New York, 2006.
(18) Hoffer, A.; Gelencser, A.; Guyon, P.; Kiss, G.; Schmid, O.; Frank, G. P.; Artaxo, P.; Andreae, M. O. Optical Properties of Humic-Like Substances (HULIS) in Biomass-Burning Aerosols. *Atmos. Chem. Phys.* **2006,** *6*, 3563–3570.
(19) Barnard, J. C.; Volkamer, R.; Kassianov, E. I. Estimation of the Mass Absorption Cross Section of the Organic Carbon Component of Aerosols in the Mexico City Metropolitan Area. *Atmos. Chem. Phys.* **2008,** *8*, 6665–6679.
(20) Rincón, A. G.; Guzmán, M. I.; Hoffmann, M. R.; Colussi, A. J. Optical Absorptivity versus Molecular Composition of Model Organic Aerosol Matter. *J. Phys. Chem. A* **2009,** *113*, 10512–10520.
(21) Guzmán, M. I.; Colussi, A. J.; Hoffmann, M. R. Photoinduced Oligomerization of Aqueous Pyruvic Acid. *J. Phys. Chem. A* **2006,** *110*, 3619–3626.
(22) Salma, I.; Ocskay, R.; Lang, G. G. Properties of Atmospheric Humic-Like Substances—Water System. *Atmos. Chem. Phys.* **2008,** *8*, 2243–2254.
(23) Sun, H. L.; Biedermann, L.; Bond, T. C. Color of brown carbon: A model for ultraviolet and visible light absorption by organic carbon aerosol. *Geophys. Res. Lett.* **2007,** *34*, L17813, DOI: 10.1029/2007gl029797 .
(24) Bergström, R. W.; Pilewskie, P.; Russell, P. B.; Redemann, J.; Bond, T. C.; Quinn, P. K.; Sierau, B. Spectral Absorption Properties of Atmospheric Aerosols. *Atmos. Chem. Phys.* **2007,** *7*, 5937–5943.
(25) Chan, M. N.; Chan, A. W. H.; Chhabra, P. S.; Surratt, J. D.; Seinfeld, J. H. Modeling of Secondary Organic Aerosol Yields from Laboratory Chamber Data. *Atmos. Chem. Phys.* **2009,** *9*, 5669–5680.
(26) Kroll, J. H.; Seinfeld, J. H. Chemistry of Secondary Organic Aerosol: Formation and Evolution of Low-Volatility Organics in the Atmosphere. *Atmos. Environm.* **2008,** *42*, 3593.
(27) Goss, K. U. Predicting Adsorption of Organic Chemicals at the Air—Water Interface. *J. Phys. Chem. A* **2009,** *113*, 3593–3624.
(28) Davidovits, P.; Kolb, C. E.; Williams, L. R.; Jayne, J. T.; Worsnop, D. R. Mass Accommodation and Chemical Reactions at Gas—Liquid Interfaces. *Chem. Rev.* **2006,** *106*, 1323–1354.
(29) Baigrie, L. M.; Cox, R. A.; Slebockatilk, H.; Tencer, M.; Tidwell, T. T. Mechanistic Studies in Strong Acids. 10. Acid-Catalyzed Enolization and Aldol Condensation of Acetaldehyde. *J. Am. Chem. Soc.* **1985,** *107*, 3640–3645.
(30) Shapiro, E. L.; Szprengiel, J.; Sareen, N.; Jen, C. N.; Giordano, M. R.; McNeill, V. F. Light-Absorbing Secondary Organic Material Formed by Glyoxal in Aqueous Aerosol Mimics. *Atmos. Chem. Phys.* **2009,** *9*, 2289–2300.
(31) Noziére, B.; Dziedzic, P.; Cordova, A. Products and Kinetics of the Liquid-Phase Reaction of Glyoxal Catalyzed by Ammonium Ions (NH_4^+) *J. Phys. Chem. A* **2009,** *113*, 231–237.
(32) Altieri, K. E.; Seitzinger, S. P.; Carlton, A. G.; Turpin, B. J.; Klein, G. C.; Marshall, A. G. Oligomers Formed through In-Cloud Methylglyoxal Reactions: Chemical Composition, Properties, and Mechanisms Investigated by Ultra-High Resolution FT-ICR Mass Spectrometry. *Atmos. Environ.* **2008,** *42*, 1476–1490.
(33) Corrigan, A. L.; Hanley, S. W.; Haan, D. O. Uptake of Glyoxal by Organic and Inorganic Aerosol. *Environ. Sci. Technol.* **2008,** *42*, 4428–4433.
(34) De Haan, D. O.; Corrigan, A. L.; Tolbert, M. A.; Jimenez, J. L.; Wood, S. E.; Turley, J. J. Secondary Organic Aerosol-Forming Reactions of Glyoxal with Amino Acids *Environ. Sci. Technol.* **2009,** *43*, 2818–2824.
(35) Kalberer, M.; Paulsen, D.; Sax, M.; Steinbacher, M.; Dommen, J.; Prevot, A. S. H.; Fisseha, R.; Weingartner, E.; Frankevich, V.; Zenobi, R.; Baltensperger, U. Identification of Polymers As Major Components of Organic Aerosol. *Science* **2004,** *303*, 1659–1662.
(36) Benson, S. W. *Thermochemical Kinetics*, 2nd ed.; Wiley: New York, 1976.
(37) Bailly, F.; Longo, G. Biological Organization and Anti-entropy. *J. Biol. Syst.* **2009,** *17*, 63–96.
(38) Brittin, W.; Gamow, G. Negative Entropy and Photosynthesis. *Proc. Natl. Acad. Sci. U.S.A.* **1961,** *47*, 724–730.
(39) Calvert, J.; Pitts, J. N. *Photochemistry*; Wiley: New York, 1966.
(40) Wexler, A. S.; Clegg, S. L. Atmospheric Aerosol Models for Systems Including the Ions H^+, NH_4^+, Na^+, SO_4^{2-}, NO_3^-, Cl^-, Br^- and H_2O *J. Geophys. Res.* 2002, *107*, art. no. 4207.
(41) Tong, C. H.; Clegg, S. L.; Seinfeld, J. H. Comparison of Activity Coefficient Models for Atmospheric Aerosols Containing Mixtures of Electrolytes, Organics, and water. *Atmos. Environ.* **2008,** *42*, 5459–5482.
(42) Guzmán, M. I.; Colussi, A. J.; Hoffmann, M. R. Photogeneration of Distant Radical Pairs in Aqueous Pyruvic Acid Glasses. *J. Phys. Chem. A* **2006,** *110*, 931–935.
(43) Guzmán, M. I.; Hoffmann, M. R.; Colussi, A. J. Photolysis of Pyruvic Acid in Ice: Possible Relevance to CO and CO_2 Ice Core Record Anomalies *J. Geophys. Res.-Atmos.* 2007, *112*, DOI:10.1029/2006jd007886.
(44) Casale, M. T.; Richman, A. R.; Elrod, M. J.; Garland, R. M.; Beaver, M. R.; Tolbert, M. A. Kinetics of Acid-Catalyzed Aldol Condensation Reactions of Aliphatic Aldehydes. *Atmos. Environ.* **2007,** *41*, 6212–6224.
(45) Noziére, B.; Dziedzic, P.; Cordova, A. Formation of Secondary Light-Absorbing "Fulvic-like" Oligomers: A Common Process in Aqueous and Ionic Atmospheric Particles? *Geophys. Res. Lett.* 2007, *34*, DOI: L21812 10.1029/2007gl031300.
(46) Noziére, B.; Esteve, W. Light-Absorbing Aldol Condensation Products in Acidic Aerosols: Spectra, Kinetics, and Contribution to the Absorption Index. *Atmos. Environ.* **2007,** *41*, 1150–1163.
(47) Patai, S. *The Chemistry of the Hydroxyl Group*; Patai, S., Ed.; Wiley: London, 1971; Vol. 2.
(48) Minerath, E. C.; Casale, M. T.; Elrod, M. J. Kinetics Feasibility Study of Alcohol Sulfate Esterification Reactions in Tropospheric Aerosols. *Environ. Sci. Technol.* **2008,** *42*, 4410–4415.

DOI: 10.1021/jz900186e | *J. Phys. Chem. Lett.* **2010,** *1*, 368–373

(49) Kropp, P. J.; Reardon, E. J.; Gaibel, Z. L. F.; Williard, K. F.; Hattaway, J. H. Photochemistry of Alkenes-Direct Irradiation in Hydroxylic Media. *J. Am. Chem. Soc.* **1973,** *95*, 7058–7067.
(50) Hashem, A. I.; Senning, A.; Hamad, A. S. S. Photochemical Transformations of 2(5H)-Furanones: A Review. *Org. Prep. Proced. Int.* **1998,** *30*, 401–425.
(51) Smith, M. B.; March, J. *Advanced Organic Chemistry, Reactions, Mechanisms and Structure*, 5th ed.; Wiley: New York, 2001.
(52) Breitmaier, E.; Voelter, W. *Carbon-13 NMR Spectroscopy: High-Resolution Methods and Applications in Organic Chemistry and Biochemistry*, 3rd ed.; VCH: New York, 1987.
(53) Frank, O.; Hofmann, T. Characterization of Key Chromophores Formed by Nonenzymatic Browning of Hexoses and L-Alanine by Using the Color Activity Concept. *J. Agric. Food Chem.* **2000,** *48*, 6303–6311.
(54) Jacquemin, D.; Perpete, E. A.; Ciofini, I.; Adamo, C. Accurate Simulation of Optical Properties in Dyes. *Acc. Chem. Res.* **2009,** *42*, 326–334.
(55) Marley, N. A.; Gaffney, J. S.; Castro, T.; Salcido, A.; Frederick, J. Measurements of Aerosol Absorption and Scattering in the Mexico City Metropolitan Area during the MILAGRO Field Campaign: A Comparison of Results from the T0 and T1 Sites. *Atmos. Chem. Phys.* **2009,** *9*, 189–206.
(56) Paredes-Miranda, G.; Arnott, W. P.; Jiménez, J. L.; Aiken, A. C.; Gaffney, J. S.; Marley, N. A. Primary and Secondary Contributions to Aerosol Light Scattering and Absorption in Mexico City during the MILAGRO 2006 Campaign. *Atmos. Chem. Phys.* **2009,** *9*, 3721–3730.

DOI: 10.1021/jz900186e | *J. Phys. Chem. Lett.* **2010,** *1*, 368–373